NORDDESIGN CONFERENCE
REYKJAVIK, ICELAND, 12-14 AUGUST 2024

3D Printing Gelatin Ultrasound Phantoms: Observations, Challenges and Future Research

Ole S. Nesheim[1], Torjus L. Steffensen[2], Martin Steinert[1], Christer W. Elverum[1]

[1]Department of Mechanical and Industrial Engineering, Norwegian University of Science and Technology
[2]Department of Circulation and Medical Imaging, Norwegian University of Science and Technology

Abstract: Ultrasound phantoms, traditionally made by casting, will not provide the geometric complexity demanded from real-life biological features, especially when internal structures are present. Also, producing patient specific models for pre-operative planning will require custom made casting molds for every case. Gelatin is regarded as the ideal material for producing phantoms for ultrasound training, however, this will dry out, rot or get damaged soon after production, making production of fresh models on-demand highly needed. Thus, we propose a low-cost AM tool based on an existing 3D printer design for producing gelatin phantoms directly. An iterative process revealed an ideal printing path for hydrogel models. Three samples were manufactured, and their quality assessed through dimensional measurement and ultrasound imaging. Dimensional accuracy varied from 1.5mm to 2.5mm. Ultrasound imaging revealed that the models possessed suitable acoustic properties but needed a reduction of air bubbles in the material. The main recommendations for future improvement were material degassing directly in the printer and improved path planning in the slicer.

Keywords: Additive Manufacturing, 3D Printing, Biomedical Design, Gelatin, Ultrasound Imaging

1 Introduction

Ultrasound imaging is growing in importance as a medical imaging modality, driven by its non-invasive nature, improving availability (Stewart et al., 2020), and the introduction of ultrasound guidance in standard procedures such as vascular punctures and needle biopsies (Franco-Sadud et al., 2019; Veltri et al., 2017). The increasing use of ultrasound has increased the need for ultrasound imaging phantoms. A phantom is an object that embodies tissue-like physical properties in some relevant aspect, such as its acoustic properties, or replicates an anatomical structure. Ultrasound imaging phantoms are used for calibrating equipment (Culjat et al., 2010), demonstrating imaging technique (Hocking et al., 2011; Kim, 2016), practicing hand-eye coordination during vascular punctures and biopsies (Vieira et al., 2013), and can be used during surgical planning (Garcia et al., 2017; Wang et al., 2017). Creating phantoms that are fit for each of these disparate purposes places several requirements on the equipment designer. The advent and flourishing of inexpensive and widely available additive manufacturing (AM) technology is becoming an important tool for complex phantom design and manufacturing.

Complex anatomy can be replicated using AM techniques. Previous work has demonstrated creating high resolution molds through AM which are then used to cast structures of interest using tissue-mimicking materials (Al-Zogbi et al., 2021; Dong et al., 2020; Huber et al., 2023; Maneas et al., 2018). Casting has several benefits, primarily accurate control over material homogeneity in the finished part, which is important for controlling the resulting image.

Printing phantoms directly using AM instead of casting would involve fewer production steps. Models might also be rapidly created on-site as needed. Certain complex shapes may be easier to reproduce accurately through direct AM because of the high design freedom allowed by AM techniques, which make it a suitable tool for manufacturing biological features. In addition, the layer wise model build process of AM has the potential to simplify designs incorporating internal structures such as vasculature, biopsy targets and foreign bodies, both for training and education or for replicating patient-specific anatomy from imaging data (Otton et al., 2017).

Tissue-mimicking phantoms can be printed directly for hard tissues such as bone (Beaulieu et al., 2019) but soft tissues are more challenging. Common materials for ultrasound phantoms are polymers like siloxanes (Yunker et al., 2013), paraffin gel waxes (Cabrelli et al., 2017; Maneas et al., 2018; Steffensen et al., 2022; Vieira et al., 2013), or hydrogels such as polyvinyl alcohol (PVA) (Culjat et al., 2010) or gelatin (Bude and Adler, 1995; Culjat et al., 2010). Gelatin is attractive because it is inexpensive, easily available and simple to process, its mechanical properties can be made to mimic those of a range of human tissues, and its acoustic properties approximately match the average of several gross tissues in the body, which are commonly used to calibrate ultrasound imaging systems (Culjat et al., 2010; Zell et al., 2007). It is also biodegradable and has some limited reusability. A major downside of gelatin is lack of durability; if not properly stored, phantoms will desiccate or spoil, and gelatin is easily torn during handling. The low material cost and limited durability of finished products motivates creating models as needed, ideally close to where they are required.

Several AM methods for producing hydrogel models have been reported (Liu et al., 2021), including inkjet (Negro et al., 2018), direct ink writing (Zhang et al., 2022), and material extrusion (Zhang et al., 2021). Material extrusion AM (commonly referred to as 3D printing) is a technology based on extruding melted material through a heated nozzle in computer-controlled paths, ultimately producing a three-dimensional model. Accordingly, the main criteria for materials used for this production method is the ability to be melted and solidified into a structure capable of carrying its own weight. Since gelatin possesses this property, it is suitable for material extrusion. Some applications of material extrusion of hydrogels (or extrusion-based bioprinting) are tissue engineering (Jang et al., 2018) and soft robotics (Heiden et al., 2022). Purpose-made extrusion-based bioprinter equipment, however, is often prohibitively expensive. In response to this issue, several low-cost bioprinter designs have been presented, typically as modifications to commercial desktop FDM printers (Fanucci and Prinsloo, 2023; Kahl et al., 2019; Roehm and Madihally, 2017). Stein et al., (2015) did some valuable work in this field, focusing on the repeatability and resolution of printing the gelatin model. These models were made through 3D printing using a robotic arm and verified by optical coherence tomography (OCT) for measuring layers.

This article will present a proof-of-concept design of a low-cost 3D printing tool (a gelatin printer) along with an iterative approach to finding a suitable slicing technique for printing successful gelatin models used for ultrasound imaging. We will investigate the preparation and production of phantoms and discuss the quality of the model based on dimensional accuracy and ultrasound imaging results. We identify and discuss parameters of particular interest for future experimental work on this topic and conclude by suggesting future research directions.

Method

Gelatin printer design

A Prusa i3 MK2S 3D printer was modified for printing hydrogels. This was done by replacing the existing extruder for printing polymers with a custom-made syringe extruder (Figure 1).

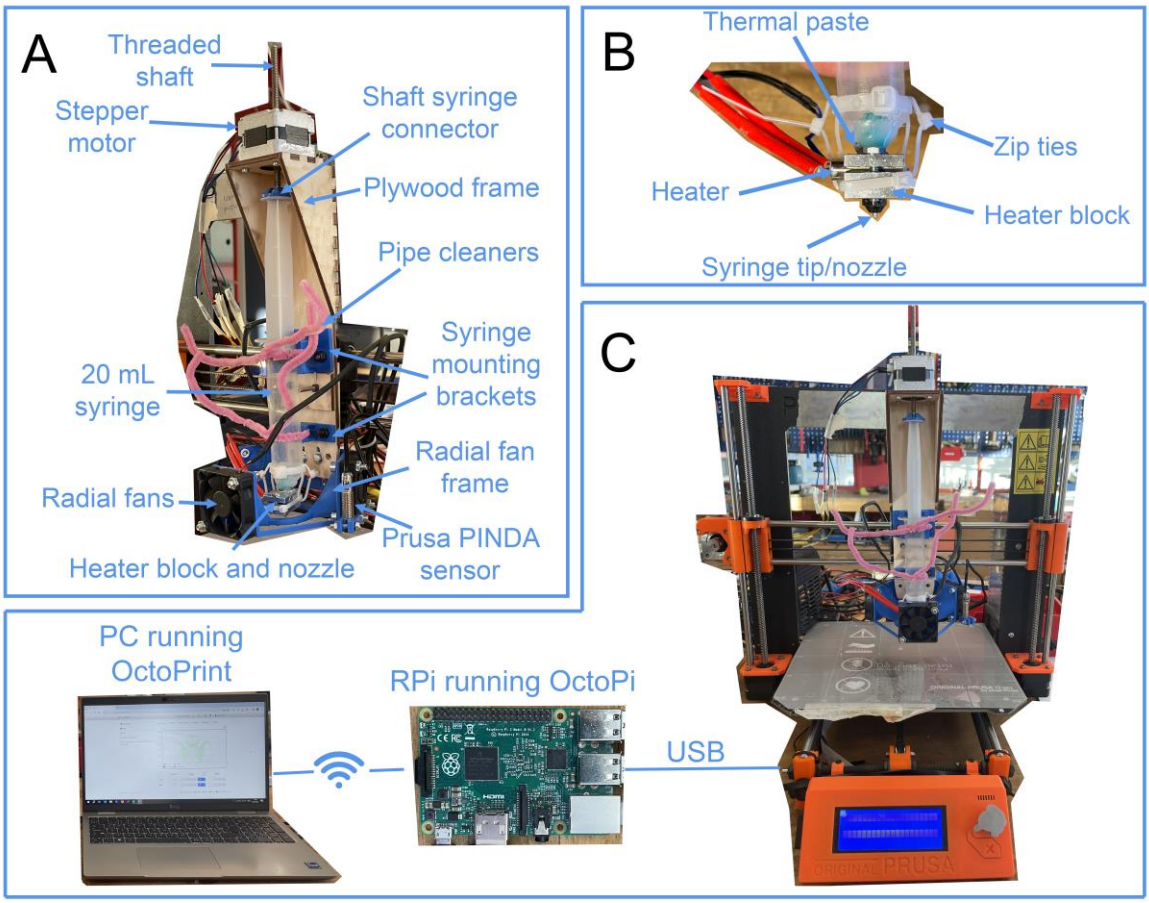

Figure 1. Printer design overview (**A**) Extruder construction (**B**) Hot-end assembly (**C**) Printer control overview

A 20ml syringe was mounted to a frame made from laser-cut 3mm plywood using 3D printed brackets held in place with metal wire (pipe cleaners). The syringe nozzle was replaced with a needle tip with an extrusion diameter of 0.9mm. The tip was fastened and sealed to the syringe with an adhesive. The metal needle tip was passed through the Prusa hot-end

heating block with a layer of thermal paste to heat up material inside the nozzle. The hot-end was then fixed to the syringe with zip ties.

To extrude material, a 0.4A 1.8° resolution stepper motor (39BYGL215A, Wantai Motor, China) was mounted on top of the plywood frame. The printer configuration file was edited to match the extruder motor's current level and extrusion speed. From the stepper motor, a 100mm threaded shaft pushed on the syringe plunger through the 3D printed shaft syringe connecter, enabling accurate control over the extrusion of the hydrogel.

Three radial fans mounted to a 3D printed frame at the bottom of the extruder provided material cooling after extrusion. A PINDA sensor (Prusa Research, Czechia) was attached to the fan-frame for bed levelling of the custom extruder. The print bed was covered with polyester sheet cut to size. The heated nozzle, stepper motor, radial fans and PINDA sensor were controlled via a common controller board (Mini-Rambo 1.3a, Prusa Research, Czechia). A Raspberry Pi 2 Model B V1.2 (Raspberry Pi Ltd, Cambridge, England) computer running OctoPi control software (Häußge, 2023) was connected to the Mini-Rambo board via USB. A separate computer running OctoPrint communicated with the Raspberry Pi via local networking. OctoPrint is a popular open-source software for controlling 3D printers, allowing significant user control and advanced tooling. Printer and slicer configuration files are available online at DOI: 10.5281/zenodo.10655480.

Sample preparation and production

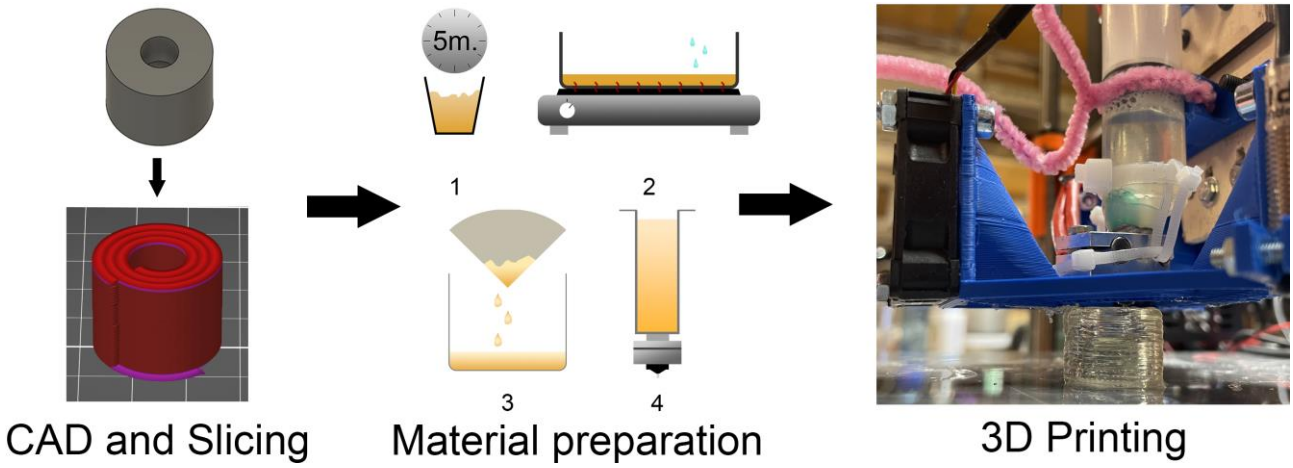

Figure 2. Sample production overview. Left: Material preparation consisting of blooming, heating, straining and transferring to printer reservoir. Middle: CAD model and slicing. Right: 3D printing

Sample production consisted of material preparation, sample design, slicing and 3D printing (Figure 2). Gelatin material was prepared as follows: to three parts cold water, one part powdered gelatin (200-250 bloom) was added and mixed in a plastic container. The gelatin was left for five minutes to bloom. Blooming is a process where gelatin is allowed to swell in cold water before heat-based dissolution and is necessary to produce a clear gel without lumps. After blooming, the water-gelatin mixture was melted at around 80°C. Next, one drop of detergent (Renax Zalo Profesjonell Ultra, Lilleborg, Oslo, Norway) per 50g of gelatin mix was added to reduce the viscosity of the liquid gelatin (Stainsby et al., 1954). The resulting mixture was then strained through a coffee filter to remove lumps or undissolved gelatine before being poured into the syringe reservoir.

Figure 3. Three samples testing various features. 1: Thin-walled structure. 2: Solid structure. 3: Solid and thick-walled structure

Three sample geometries (Figure 3) were designed and printed to assess 3D printing of thin- and thick-walled structures as well as solids. These features were of interest as representative of a few fundamental requirements for producing more complex structures. Sample 1 was a thin-walled cylinder; sample 2 was a solid cylinder; sample 3 was a combination

geometry featuring a solid cylinder bottom and a thick-walled annulus on top, resulting in a partial cavity. One of each sample were manufactured. Dimensional accuracy of the finished models were measured using a caliper and compared to the CAD of sample nr. 3.

Slicing technique

SuperSlicer, a forked version of Slic3r, based on PrusaSlicer was used to generate the g-code because of its excellent capability of customizing print parameters. Some important print parameters are listed below in Table 1.

Table 1. Print parameters used during sample production

Nozzle temperature	50° C
Bed temperature	20° C (Room temperature)
Layer height	0.5 mm
Print speed	6 mm/s
Extrusion width	2.1073 mm
Infill spacing	2 mm
Infill	Sample 1: 0% Sample 2 and 3: 100%
Perimeters	Sample 1: 1 Sample 2 and 3: 0

The nozzle was heated to 50°C to reduce clogging in the needle tip as material was extruded relatively slowly near the cooling fans. The first thin-walled hollow cylinder was printed using a single perimeter and "Spiral vase", and the other figures were sliced with 100% infill and no perimeter. The optimal infill pattern was found using an iterative approach. All three iterations are visualized in Figure 4.

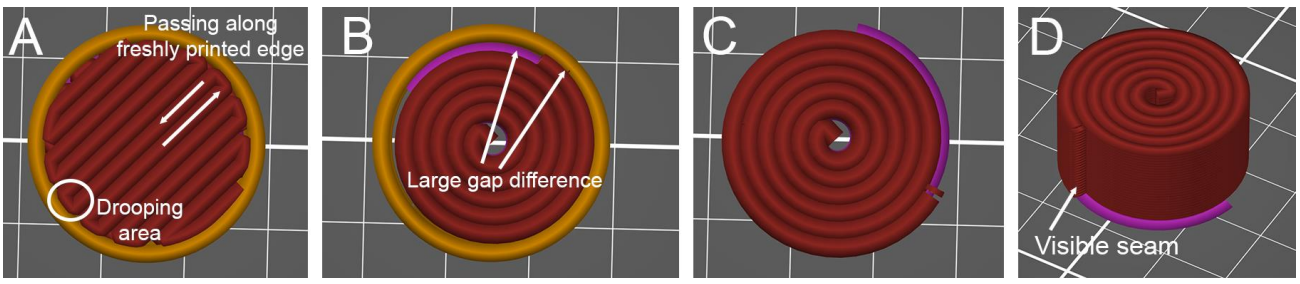

Figure 4. Infill iterations. A: 1st iteration – Single perimeter with rectilinear infill. B: 2nd iteration – Single perimeter with Archimedean Chords infill. C and D: 3rd iteration – No perimeter with Archimedean Chords infill.

One key lesson from the first iteration (Figure 4A) was that due to the reduction of sudden shifts in printing direction in the corners of the Rectilinear infill, the nozzle was forced to brush against freshly deposited material before solidification (hereby referred to as nozzle drag-by). This material may have solidified at the nozzle tip, clogging the nozzle and destroying the model. In addition, the 180° turns at the edges of the infill pattern produced a drooping excess gelatin area, possibly due to the extrusion speed not matching the deceleration of the print head at the edge before turning around, ultimately leading to over-extrusion at the edges. The root of this issue may have been the slow retraction response of the syringe compared to a traditional polymer extruder, which after all, the slicer configuration is adapted to. Both these main issues were addressed in the second iteration (Figure 4B) by switching from Rectilinear infill to Archimedean Chords. Printing in spiral shapes yielded the most stable results as both edge drooping and nozzle drag-by were reduced. However, due to the poor retraction properties of the syringe, start, stop, lift, and travel motions produced excess droop. This excess material was most problematic when traveling across the deposited layer as it interfered with the next layer. These movements were triggered mainly between the perimeter and infill. The spiral also generated minimum and maximum diameters, causing a significant gap difference (Figure 4B) between infill and perimeter, producing a slight material

overlap that was problematic for succeeding layers. These issues were fixed by removing the perimeter and only extruding the Archemedian Chords infill. Sadly, removing the perimeter made the vertical seam more visible (Figure 4D).

Ultrasound imaging

Ultrasound imaging is based on transmission and reflection of acoustic waves through a material. Images are generated based on the reflected energy of acoustic pulses emitted in a phased transducer array, with flight time determining depth and relative intensity interpreted as brightness. Wave reflection at the interface between two materials is determined by their different acoustic impedance, described by the reflection coefficient R:

$$R = \left(\frac{Z_2 - Z_1}{Z_2 + Z_1}\right)^2$$

Where Z is the acoustic impedance of the materials, proportional to the material density and the local speed of sound, which in turn is proportional to stiffness. When designing tissue-mimicking phantoms, designers can use materials of differing impedance to vary the echogenicity of the section being examined, resulting in the desired image. As R depends on local speed of sound, the inclusion of regions with very different impedance, such as air, in a phantom medium is undesirable. The large difference in acoustic impedance means most of the wave energy is reflected, causing a bright region to appear in the image with a characteristic “shadow” below it in the image, hindering imaging in this region.

A good tissue-mimicking material, therefore, needs to be as clear of air bubbles as possible as a starting point for the design process. To assess the imaging quality of the directly-printed gelatin structures, the 3D printed samples were immersed in a water bath (Figure 5). B-mode imaging took place in situ immediately after printing and cooling, using a handheld ultrasound imaging device (Vscan Dual Probe, GE Healthcare). Each sample was, in turn, imaged cross-sectionally, with gain adjusted as necessary.

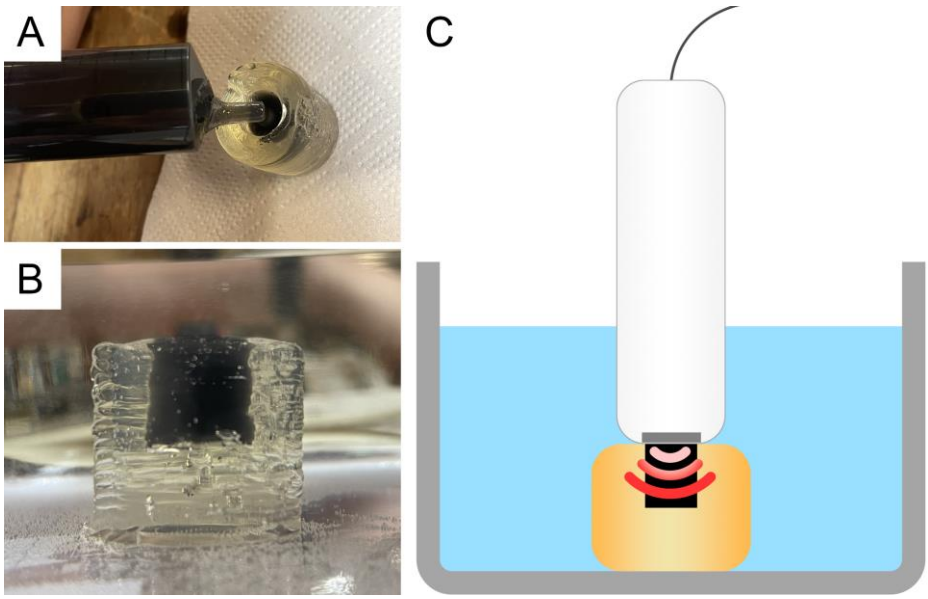

Figure 5. A: Inserting gelatin with black pigment powder. B: Sample nr. 3 with doped gelatine insert submerged under water. C: Schematic ultrasound imaging setup.

The thick-walled sample was first investigated as printed, then filled with a mixture of gelatin containing a powdered pigment to act as a dopant for improved echogenicity, and then re-investigated. This inclusion was intended to simulate a hyperechoic region inside a larger structure, an interesting case in ultrasound-guided needle biopsy.

Results

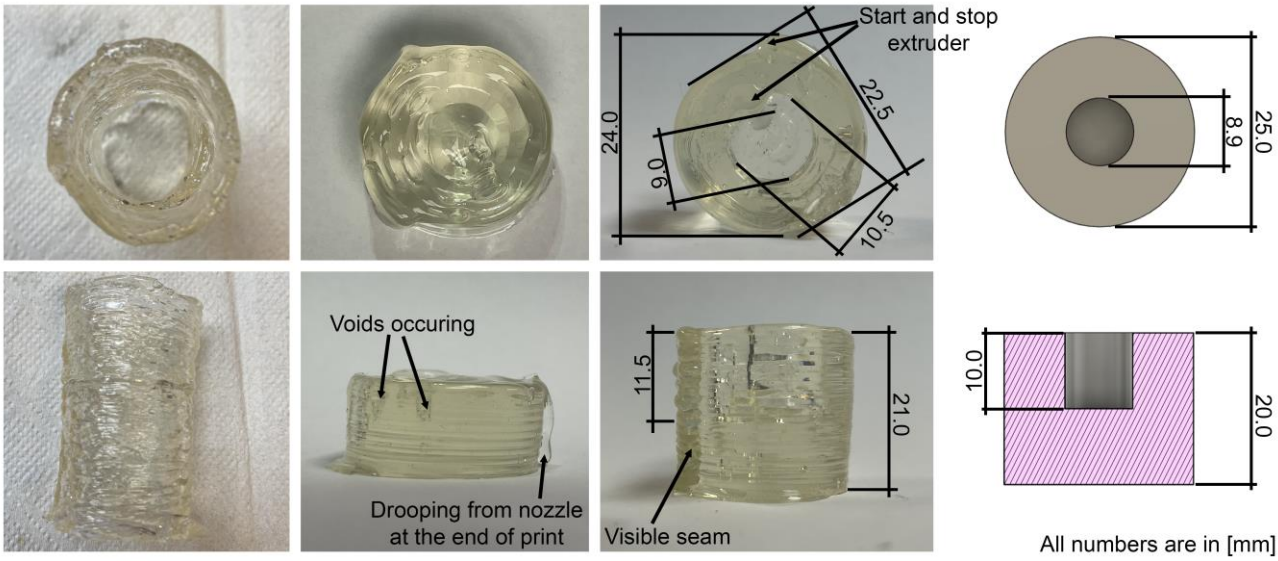

Figure 6. From left to right: Printed sample 1, 2, 3 and CAD model of sample 3

Printed samples are shown in Figure 6. First, the total model height in the CAD was measured to 21.0mm. The 10.0mm deep internal hole was measured to 11.5mm giving a maximum deviation of 1.5mm. The outer diameter varied from 22.5mm to 24.0mm compared to the CAD file with 25.0mm. The inner diameter was measured to be 9.0mm and 10.5mm compared to the CAD model with a diameter of 8.9mm. All measurements were within a maximum deviation of 2.5mm. The main reason for the variation was due to the Archimedean Infill and lacking perimeter. I.e., the infill combined with the 2mm extrusion width gave a visible start and stop (pointed out on sample 3) ultimately resulting in a maximum and minimum diameter. I.e., the same variation occurred in the slicer (Figure 4D). Dimensional accuracy may therefore be improved by experimenting with infill pattern. By ignoring dimensional inaccuracies caused by the slicer, the maximum measured offset was 1.5mm.

Another note on the dimensions is that the outer diameter is too small, and the inside diameter is too big compared to the CAD model due to the lacking perimeter. Another clear visual aspect was the visible seam clearly seen in sample 3. This issue may be addressed by placing seam randomly instead of in a line. Also in this case, a clear perimeter may also help reducing the visibility of the seam. In sample 2, some unintentional voids originated during printing. These were also observed during printing and was caused by the extruded material losing contact with the previously deposited layer. This discrepancy may be caused by mechanical inaccuracies of the machine or a slightly too high layer height. Finally, some drooping occurred on the side of each sample. This was simply caused by the nozzle not being properly removed at the end of the g-code, resulting in some excess material running onto the sample.

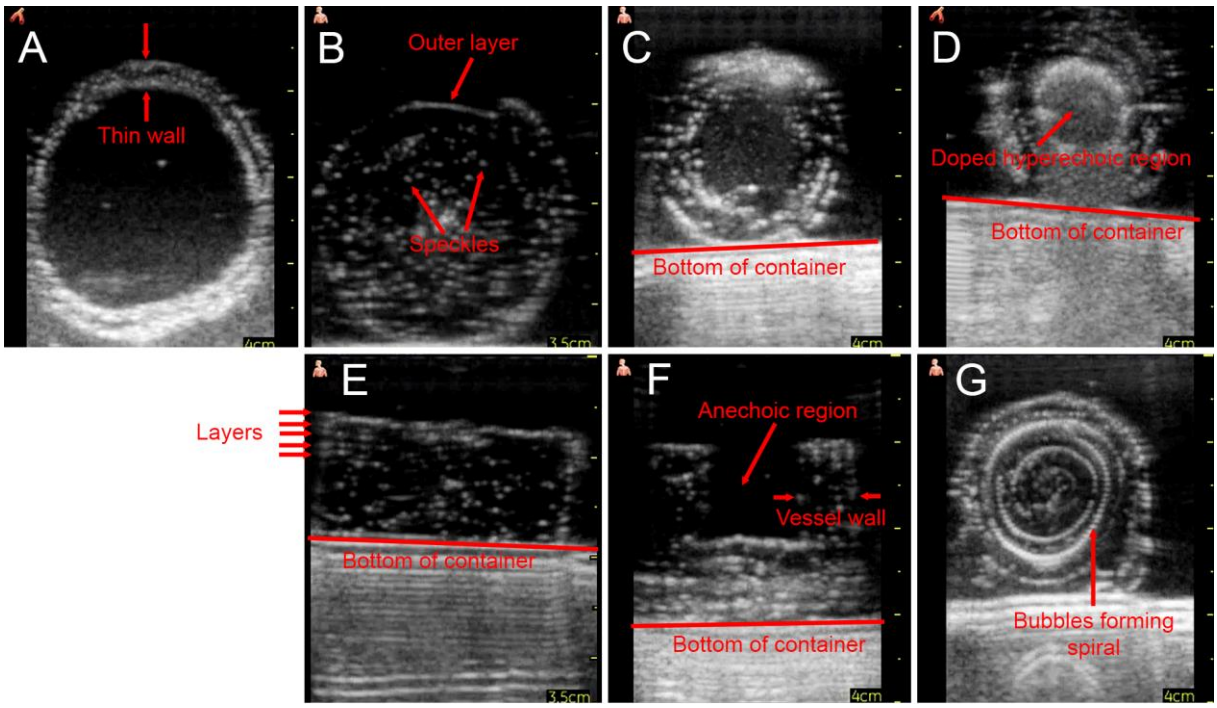

Figure 7. Ultrasound images. A: Sample 1. B and E: Sample 2. C and F: Sample 3. D: Sample 3 after added gelatin with black pigment. G: Bottom layer of sample 3

Figure 7 shows ultrasound images of the samples as printed. All the printed structures are recognizable in the B-mode images, with distinct surface boundaries. The internal regions are characterized by a general anechoic or hypoechoic background, consistent with a homogeneous hydrogel, but with a distinct bright speckle pattern. We hypothesize these speckles to mainly be caused by the inclusion of air bubbles in the gelatin prints. This would also explain the "shadow" artifacts visible in some of the views.

The thin-walled annular structure of sample 1 is clearly identifiable (Figure 7A). Figure 7B shows the top view of sample 2, demonstrating the internal speckle pattern. Figure 7E showing the same sample from the side, indicates that in certain areas layer transitions caused by the printing process are also visible. The top view of sample 3 without the added inclusion can be seen in Figure 7C. The anechoic region in the center of the phantom is visible but contains some shadowing likely caused by the air content in the thick wall. A side view of the same sample (Figure 7F) shows no echo in the same region when not imaged through the thick wall. The doped inclusion can be seen as a hyperechoic region in Figure 7D, albeit with an even more distinct shadow artifact. Bubbles tracing the spiral infill pattern of sample 3, clearly visible in Figure 7G, were observed during printing. Air bubbles trapped at the end of the nozzle were extruded in concert with the infill pattern, resulting in the visible spiral. Speckles following the spiral infill can also be seen (although not as clearly) in Figure 7B, 7C and 7D. The speckles in Figure 7F are also clearest in the bottom of the figure (i.e., the solid part) and seems to be following the layer lines.

Discussion and future work

Ultrasound imaging clearly showed impurities – probably air bubbles, gelatin impurities or a combination of both – trapped within the printed structure, compromising the quality of the samples. The speckles seem to follow the printing pattern and layers, indicating that they were present already in the syringe. 3D printing as a production method is inherently prone to producing anisotropic components due to the layer wise buildup of the model. Thermal differences between newly deposited material and the previous layer may lead to inadequate layer fusion. In this case each deposited string interfaces with other strings, whereas in casting the melted material only interfaces with the edge of the casting mold. Impurities or air can then interfere with the material in-between strings. This makes casted models normally more isotropic in its properties than 3D printed models. This issue is common in 3D printing of traditional plastic polymers. Some existing solutions are post annealing (Torres et al., 2015) and in-situ layer heating (Lee et al., 2021). An adaption of these solutions to printing gelatin is not yet tested, but additional heating may help reduce the layer visibility in the ultrasound images. Bubbles may be eliminated by degassing the material in a vacuum chamber while contained in the printer reservoir, or by improving blooming technique. Transferring the material mixture from the heating pot to printer reservoir may also have affected the air bubble content and is a procedure in need of improvement. E.g., the material can be strained directly into the reservoir, reducing the number of pouring steps. This challenge is yet to be overcome and should be an area of future research.

The speckles may also have been impurities, calling for a cleaner gelatin mixture. Conventional food grade gelatin was used for this project, but other gelatin types may also be tested and affect the purity level. Gelatins have various strengths, known as bloom number (Hanani, 2016). A higher bloom number yield a stronger and stiffer gelatin, ultimately producing a stiffer model. Gelatin hardness can also be controlled through the gelatin water ratio. Implications of raw material has also yet not been researched. Gelatin is extracted from various animal collagens such as pigs, cows or fish. Investigating bloom number, collagen type and concentration presents an exciting new field of study and should be investigated in the future and evaluated by looking at printability and ultrasound imaging.

The material may also be enhanced through other additives to achieve certain features. In this article, powdered pigment was added to one sample to simulate an inclusion. Introducing other additives to mimic various tissue, muscle, bone or other biological features should be investigated. Multimaterial printing should then be implemented to enable the integration of different materials and structures into the model. Experimenting with material mixtures will certainly affect the printability of the material. Accordingly, in concert with material experimentation, hardware aspects such as nozzle size and cooling power and print parameters such as infill width, layer height, nozzle temperature etc. should be investigated. The print parameters were a result of many iterations of printer calibration attempts. E.g., an infill spacing of 2mm is much higher than the nozzle diameter of 0.9mm. This was adjusted after the material was observed to ooze out much more than first expected. By doing more research on achieving the optimal material mix, print parameters will change accordingly. This should be researched more in the future.

Slicing techniques should be investigated further. We propose for the next iteration to aim for a print path that will first print outer perimeter and continue printing infill in the same path, ideally without any stops, lifts, or travel. In addition, the print path should not turn 180° at any point resulting in nozzle drag-by. Gaps should also be minimized. Print path optimization and infill patterns are still open and active research areas. In future work, a dedicated slicer software for printing hydrogels, as either stand-alone software or implemented in existing slicer programs such as SuperSlicer, would give designers the necessary freedom to control these parameters. Slicer software with higher path control such as FullControl GCode Designer (Gleadall, 2021) may also be a suitable alternative. This may allow the final hydrogel phantoms to be dimensionally closer to the original CAD model.

Another problem occurring after some time during printing was hydrogel solidifying in the printer reservoir. This should be fixed in the future by implementing a heated reservoir that will keep the material liquid during the entire manufacturing session.

To summarize, the key lessons learned were:

- Slicing technique and print path is crucial for successful prints: reduce sudden shifts of movement, remove travel, reduce nozzle drag-by of fresh material.
- Slicing techniques should be adapted and evaluated in terms of dimensional accuracy of the model.
- Trapped air bubbles causes interference with the ultrasonic images. Degassing the material directly inside the printer reservoir should be investigated.
- Bloom number, collagen type and gelatin concentration must be rigorously examined and evaluated in terms of printability and ultrasound image quality.
- The material reservoir should be heated so the gelatin does not set during manufacturing.

Conclusion

Ultrasound imaging phantoms may be printed directly using simple 3D printing equipment with recognizable features in the generated image. However, problems common to 3D printing introduce challenges particular to the application of these printed objects. The layer wise buildup of the model along with excessive material handling during preparation are likely to contribute to significant amounts of trapped microbubbles, and speckles reducing the ultrasound image quality. Effectively countering these problems will be necessary for adoption of this technique. We propose to investigate material degassing directly in the printer reservoir before printing to reduce the appearance of air bubbles. In future work, we will also look into heat treatments such as annealing to reduce layer visibility and better path planning to bring the finished model dimensionally closer to the CAD design. Various gelatin types should be tested and straining technique improved to remove impurities. We believe this work benefits the design community by sharing our experiences working with these materials, and hope the observations and lessons presented in this paper will contribute to the knowledge on creating better gelatin models for ultrasound imaging purposes.

References

Al-Zogbi, L., Bock, B., Schaffer, S., Fleiter, T., Krieger, A., 2021. A 3-D-Printed Patient-Specific Ultrasound Phantom for FAST Scan. Ultrasound in Medicine & Biology 47, 820–832. https://doi.org/10.1016/j.ultrasmedbio.2020.11.004

Beaulieu, A., Linden, A. zur, Phillips, J., Arroyo, L.G., Koenig, J., Monteith, G., 2019. Various 3D printed materials mimic bone ultrasonographically: 3D printed models of the equine cervical articular process joints as a simulator for ultrasound guided intra-articular injections. PLOS ONE 14, e0220332. https://doi.org/10.1371/journal.pone.0220332

Bude, R.O., Adler, R.S., 1995. An easily made, low-cost, tissue-like ultrasound phantom material. J. Clin. Ultrasound 23, 271–273. https://doi.org/10.1002/jcu.1870230413

Cabrelli, L.C., Pelissari, P.I.B.G.B., Deana, A.M., Carneiro, A.A.O., Pavan, T.Z., 2017. Stable phantom materials for ultrasound and optical imaging. Phys. Med. Biol. 62, 432. https://doi.org/10.1088/1361-6560/62/2/432

Culjat, M.O., Goldenberg, D., Tewari, P., Singh, R.S., 2010. A review of tissue substitutes for ultrasound imaging. Ultrasound Med Biol 36, 861–873. https://doi.org/10.1016/j.ultrasmedbio.2010.02.012

Dong, J., Zhang, Y., Lee, W.-N., 2020. Walled vessel-mimicking phantom for ultrasound imaging using 3D printing with a water-soluble filament: design principle, fluid-structure interaction (FSI) simulation, and experimental validation. Phys. Med. Biol. 65, 085006. https://doi.org/10.1088/1361-6560/ab7abf

Fanucci, S., Prinsloo, E., 2023. Development of a low-cost hydrogel microextrusion printer based on a Kossel delta 3D printer platform. Engineering Reports 5, e12615. https://doi.org/10.1002/eng2.12615

Franco-Sadud, R., Schnobrich, D., Mathews, B.K., Candotti, C., Abdel-Ghani, S., Perez, M.G., Rodgers, S.C., Mader, M.J., Haro, E.K., Dancel, R., Cho, J., Grikis, L., Lucas, B.P., Force, the S.P.U.T., Soni, N.J., 2019. Recommendations on the Use of Ultrasound Guidance for Central and Peripheral Vascular Access in Adults: A Position Statement of the Society of Hospital Medicine. Journal of Hospital Medicine 14, E1–E22. https://doi.org/10.12788/jhm.3287

Garcia, J., Yang, Z., Mongrain, R., Leask, R.L., Lachapelle, K., 2017. 3D printing materials and their use in medical education: a review of current technology and trends for the future. BMJ Simul Technol Enhanc Learn 4, 27–40. https://doi.org/10.1136/bmjstel-2017-000234

Gleadall, A., 2021. FullControl GCode Designer: Open-source software for unconstrained design in additive manufacturing. Additive Manufacturing 46, 102109. https://doi.org/10.1016/j.addma.2021.102109

Hanani, Z.A.N., 2016. Gelatin, in: Caballero, B., Finglas, P.M., Toldrá, F. (Eds.), Encyclopedia of Food and Health. Academic Press, Oxford, pp. 191–195. https://doi.org/10.1016/B978-0-12-384947-2.00347-0

Häußge, G., 2023. OctoPrint.org.

Heiden, A., Preninger, D., Lehner, L., Baumgartner, M., Drack, M., Woritzka, E., Schiller, D., Gerstmayr, R., Hartmann, F., Kaltenbrunner, M., 2022. 3D printing of resilient biogels for omnidirectional and exteroceptive soft actuators. Science Robotics 7, eabk2119. https://doi.org/10.1126/scirobotics.abk2119

Hocking, G., Hebard, S., Mitchell, C.H., 2011. A Review of the Benefits and Pitfalls of Phantoms in Ultrasound-Guided Regional Anesthesia. Reg Anesth Pain Med 36, 162-162–170. https://doi.org/10.1097/AAP.0b013e31820d4207

Huber, C.M., Heim, C., Ermert, H., Rupitsch, S.J., Ullmann, I., Lyer, S., 2023. Wall-less Flow Phantoms with 3D printed Soluble Filament for Ultrasonic Experiments. Current Directions in Biomedical Engineering 9, 97–100. https://doi.org/10.1515/cdbme-2023-1025

Jang, T.-S., Jung, H.-D., Pan, H.M., Han, W.T., Chen, S., Song, J., 2018. 3D printing of hydrogel composite systems: Recent advances in technology for tissue engineering. Int J Bioprint 4, 126. https://doi.org/10.18063/IJB.v4i1.126

Kahl, M., Gertig, M., Hoyer, P., Friedrich, O., Gilbert, D.F., 2019. Ultra-Low-Cost 3D Bioprinting: Modification and Application of an Off-the-Shelf Desktop 3D-Printer for Biofabrication. Frontiers in Bioengineering and Biotechnology 7.

Kim, Y.H., 2016. Ultrasound Phantoms to Protect Patients from Novices. Korean J Pain 29, 73–77. https://doi.org/10.3344/kjp.2016.29.2.73

Lee, J.E., Park, S.J., Son, Y., Park, K., Park, S.-H., 2021. Mechanical reinforcement of additive-manufactured constructs using in situ auxiliary heating process. Additive Manufacturing 43, 101995. https://doi.org/10.1016/j.addma.2021.101995

Liu, C., Xu, N., Zong, Q., Yu, J., Zhang, P., 2021. Hydrogel prepared by 3D printing technology and its applications in the medical field. Colloid and Interface Science Communications 44, 100498. https://doi.org/10.1016/j.colcom.2021.100498

Maneas, E., Xia, W., Nikitichev, D.I., Daher, B., Manimaran, M., Wong, R.Y.J., Chang, C.-W., Rahmani, B., Capelli, C., Schievano, S., Burriesci, G., Ourselin, S., David, A.L., Finlay, M.C., West, S.J., Vercauteren, T., Desjardins, A.E., 2018. Anatomically realistic ultrasound phantoms using gel wax with 3D printed moulds. Phys Med Biol 63. https://doi.org/10.1088/1361-6560/aa9e2c

Negro, A., Cherbuin, T., Lutolf, M.P., 2018. 3D Inkjet Printing of Complex, Cell-Laden Hydrogel Structures. Sci Rep 8, 17099. https://doi.org/10.1038/s41598-018-35504-2

Otton, J.M., Birbara, N.S., Hussain, T., Greil, G., Foley, T.A., Pather, N., 2017. 3D printing from cardiovascular CT: a practical guide and review. Cardiovasc Diagn Ther 7, 507–526. https://doi.org/10.21037/cdt.2017.01.12

Roehm, K.D., Madihally, S.V., 2017. Bioprinted chitosan-gelatin thermosensitive hydrogels using an inexpensive 3D printer. Biofabrication 10, 015002. https://doi.org/10.1088/1758-5090/aa96dd

Stainsby, G., Saunders, P.R., Ward, A.G., 1954. The preparation and properties of some gelatin fractions. J. Polym. Sci. 12, 325–335. https://doi.org/10.1002/pol.1954.120120127

Steffensen, T.L., Kriesi, C., Steinert, M., Lafrenz, T., Brede, J.R., Auflem, M., 2022. Ultrasound phantom. US20220304922A1.

Stein, N., Saathoff, T., Antoni, S.-T., Schlaefer, A., 2015. Creating 3D gelatin phantoms for experimental evaluation in biomedicine. Current Directions in Biomedical Engineering 1, 331–334. https://doi.org/10.1515/cdbme-2015-0082

Stewart, K.A., Navarro, S.M., Kambala, S., Tan, G., Poondla, R., Lederman, S., Barbour, K., Lavy, C., 2020. Trends in Ultrasound Use in Low and Middle Income Countries: A Systematic Review. Int J MCH AIDS 9, 103–120. https://doi.org/10.21106/ijma.294

Torres, J., Cotelo, J., Karl, J., Gordon, A.P., 2015. Mechanical Property Optimization of FDM PLA in Shear with Multiple Objectives. JOM 67, 1183–1193. https://doi.org/10.1007/s11837-015-1367-y

Veltri, A., Bargellini, I., Giorgi, L., Almeida, P.A.M.S., Akhan, O., 2017. CIRSE Guidelines on Percutaneous Needle Biopsy (PNB). Cardiovasc Intervent Radiol 40, 1501–1513. https://doi.org/10.1007/s00270-017-1658-5

Vieira, S.L., Pavan, T.Z., Junior, J.E., Carneiro, A.A.O., 2013. Paraffin-Gel Tissue-Mimicking Material for Ultrasound-Guided Needle Biopsy Phantom. Ultrasound in Medicine & Biology 39, 2477–2484. https://doi.org/10.1016/j.ultrasmedbio.2013.06.008

Wang, K., Ho, C.-C., Zhang, C., Wang, B., 2017. A Review on the 3D Printing of Functional Structures for Medical Phantoms and Regenerated Tissue and Organ Applications. Engineering 3, 653–662. https://doi.org/10.1016/J.ENG.2017.05.013

Yunker, B.E., Cordes, D., Scherzinger, A.L., Dodd, G.D., Shandas, R., Feng, Y., Hunter, K.S., 2013. An investigation of industrial molding compounds for use in 3D ultrasound, MRI, and CT imaging phantoms. Med. Phys. 40, n/a-n/a. https://doi.org/10.1118/1.4802083

Zell, K., Sperl, J.I., Vogel, M.W., Niessner, R., Haisch, C., 2007. Acoustical properties of selected tissue phantom materials for ultrasound imaging. Phys. Med. Biol. 52, N475. https://doi.org/10.1088/0031-9155/52/20/N02

Zhang, L., Lee, W., Li, X., Jiang, Y., Fang, N.X., Dai, G., Liu, Y., 2022. 3D direct printing of mechanical and biocompatible hydrogel meta-structures. Bioactive Materials 10, 48–55. https://doi.org/10.1016/j.bioactmat.2021.08.015

Zhang, Y.S., Haghiashtiani, G., Hübscher, T., Kelly, D.J., Lee, J.M., Lutolf, M., McAlpine, M.C., Yeong, W.Y., Zenobi-Wong, M., Malda, J., 2021. 3D extrusion bioprinting. Nat Rev Methods Primers 1, 1–20. https://doi.org/10.1038/s43586-021-00073-8

Contact: Ole S. Nesheim, Department of Mechanical and Industrial Engineering, Faculty of Engineering, Norwegian University of Science and Technology, Richard Birkelands vei 2B, 7034, Trondheim, Norway, ole.s.nesheim@ntnu.no